RESEARCH ARTICLE

Design and Optimization of a Novel Multi-Quadrant Spatial Array for Non-Invasive Focalized Magnetic Stimulation of the Deep Brain

XIAO FANG[1,2,3,4]**, XIAO XIANG LI**[2]**, HAI LIAN JING**[1]**, WEI LIU**[1]**, TAO ZHANG**[3,4]**, AND SHUANG ZHANG**[3,4]**, (Senior Member, IEEE)**

[1]College of Nuclear Technology and Automation Engineering, Chengdu University of Technology, Chengdu 610059, China
[2]Wuhan National High Magnetic Field Center, Huazhong University of Science and Technology, Wuhan 430074, China
[3]School of Life Science and Technology, University of Electronic Science and Technology of China, Chengdu 611731, China
[4]Clinical Hospital of Chengdu Brain Science Institute, MOE Key Laboratory for Neuroinformation, University of Electronic Science and Technology of China, Chengdu 611731, China

Corresponding author: Xiao Fang (fangxiao930106@163.com)

ABSTRACT As a non-invasive neuromodulation technique, transcranial magnetic stimulation (TMS) has shown great potential in scientific research and clinical application. Using TMS to stimulate the deep brain is important for enhancing the therapeutic effects of mental disorders and explaining the causes of mental disorders. However, the intracranial induced electric field (E-field) generated by conventional magnetic stimulation coils dissipates severely with increasing stimulation depth and the focalized stimulation is limited to superficial areas. In this paper, we first propose a novel multi-quadrant spatial array (MQS array) based on curved-shaped coils. Each coil in the MQS array is tangent to the head and bent away from the human head, which is conducive to reducing the accumulation of non-longitudinal induced E-field components and improving the stimulation focalization in the deep brain. Then, we propose a new spatial magnetic array optimization method based on the BP-NSGA-II algorithm. The predictive models of deep brain transcranial magnetic stimulation characteristics of the spatial array are obtained by the BP neural network and the multi-objective optimization of the stimulation currents applied in the spatial array is performed with the NSGA-II algorithm. Results show that the MQS array can produce an obvious focusing area at 10 cm below the scalp which satisfies the depth requirement of deep brain transcranial magnetic stimulation. Under the same constraint of Joule loss, the optimized MQS array can enhance intracranial stimulation intensity by 131%, increase the longitudinal attenuation ratio to 4.5 times, and reduce the focusing area by 76% compared to the conventional planar magnetic stimulation array. The proposed MQS array has significant advantages in deep brain focalized stimulation, and the spatial array optimization method described in this study may provide a valuable reference for coil or array optimization processes in other application contexts.

INDEX TERMS Deep brain transcranial magnetic stimulation, multi-objective optimization, stimulation focalization.

The associate editor coordinating the review of this manuscript and approving it for publication was Md. Abdur Razzaque.

I. INTRODUCTION

Transcranial magnetic stimulation (TMS) is a non-invasive neuromodulation technology that is widely employed in the treatment and scientific investigation of various mental

illnesses, including major depression and schizophrenia [1], [2], [3]. TMS can also be used in conjunction with functional magnetic resonance imaging (fMRI), positron emission tomography (PET), and electroencephalography (EEG) to examine the anatomy and function of the human brain [4], [5]. A pair of stimulation coils is often placed near the human head during TMS treatment [6], [7]. The TMS power supply system delivers pulsed currents to the stimulation coil at a specific time sequence. The time-varying currents produce alternating magnetic fields (B-field) in the space around the coil, which in turn generates an induced electric field (E-field) in the intracranial target area, causing the membrane potentials of the target neurons to change and creating a neuromodulatory effect [8], [9], [10].

The research of deep brain neuromodulation mechanisms is the key to treating mental diseases and exploring the causes of mental diseases. Precise stimulation of deep brain target areas such as the hippocampus and amygdala not only has urgent clinical application needs but also has great scientific research value [11], [12], [13], [14]. The figure-of-eight coil (FOE coil), which consists of two planar circular coils, is the most commonly used commercial TMS coil. It can activate biological tissues to a depth of 2 cm to 2.5 cm below the scalp and regulate cortical excitability [15], [16]. However, the target tissues for deep brain transcranial magnetic stimulation are usually located further than 4 cm below the scalp. For instance, as the key neural basis for the study of major depression, the ventromedial prefrontal cortex (VMPFC) region is located at a depth of 7 cm below the human scalp [17], which exceeds the effective stimulation depth of the traditional TMS coil. In addition, as the stimulation depth increases, the intracranial-induced E-field generated by conventional TMS coils diverges severely, weakening the stimulation focalization and exposing a large amount of non-target tissues to the strong stimulation, raising the risk of causing stimulation side effects.

Many studies have been undertaken in recent years on the design of TMS coils to improve the effects of deep brain transcranial magnetic stimulation. The biconical coil was one of the first deep brain coils proposed. The biconical coil can raise the stimulation depth to 3–4 cm below the human scalp as compared to the conventional FOE coil. The biconical coil's focusing area is 94.4 cm^2, which is 1.86 times greater than that of the conventional FOE coil, causing a non-negligible risk of epilepsy [18]. In 2002, Roth Y of Israel's Ben Gurion University proposed the Hesed coil family (H-coil) [6], [19], [20], [21], [22], [23]. The H-coil is a representative deep brain coil that can increase the depth of stimulation. But the increased stimulation depth of the H-coil comes at the sacrifice of stimulation focalization: the stimulation depth of the H-coil can reach 3-6cm below the scalp while the focusing volume of the H-coil is six times that of the FOE coil [24]. In 2015, the Halo coil working with two circular coils (the HTC coil) was proposed by Lu Mai et al. from Lanzhou Jiaotong University in China. The HTC coil can raise the longitudinal attenuation ratio to 2.07,

which is advantageous for improving the effects of deep brain transcranial magnetic stimulation [25]. In 2019, Rastogiet al. proposed the multi-coil configuration called the Triple Halo Coil (THC) which could stimulate deep regions of the brain with more than 7 times higher magnetic field at a depth of 10 cm as compared with the FOE coil but the stimulation focalization in the deep brain was not discussed [26].

The main contributions of this paper are given as follows:

●(1) The multi-quadrant spatial array (MQS array) with a unique geometric structure is proposed to realize non-invasive focused stimulation in the deep brain.

●(2) The BP-NSGA-II algorithm-based optimization method is proposed to achieve multi-objective optimization of the stimulation currents applied in TMS arrays.

●(3) The performance of the optimized MQS array was evaluated by analyzing three important characteristics of induced E-field in the deep brain. A conventional TMS array was compared to the optimized MQS array under the same Joule power loss to prove the advantages of the MQS array design.

In this paper, the authors propose a design of a stimulation array with an innovative spatial structure and an optimization method based on a hybrid algorithm to improve the stimulation performance of TMS in the deep brain. The study is organized as follows: Section I introduces the research background and purpose. Section II describes the geometry of the MQS array in detail and explains the principle of the MQS array. Section III presents the 3D finite element numerical models including the MQS array, the human head, and their meshes during finite element numerical calculation. Section IV introduces the structure of the multi-objective optimization method, and the optimization steps and provides the optimized results. Section V compares the spatial distributions of intracranial induced E-field generated by an optimized MQS array and the conventional TMS coil under the constraint of identical Joule power loss. Section VI concludes the work and presents some future works.

## II. DESCRIPTION OF THE MQS ARRY
A. GEOMETRY OF THE MQS ARRAY

The MQS array proposed in this study is different from conventional single-layer or multi-layer TMS arrays, which usually consist of planar circular coils, while the MQS array consists of multiple curved coils that are placed at specific spatial locations.

A 3D model of the MQS array is shown in Fig 1(a). In the MQS array, eight quadrantal coils with identical geometric characteristics are distributed separately among the eight quadrants of the 3D coordinate space system. The center point of the human head is set as the origin of the space coordinate system. The coils are referred to as I-coil, II-coil, III-coil, IV-coil, V-coil, VI-coil, VII-coil, and VIII-coil based on their relative location to the human head. Fig. 1(b) and Fig. 1(c) show the vertical view and side view of the MQS array, respectively.
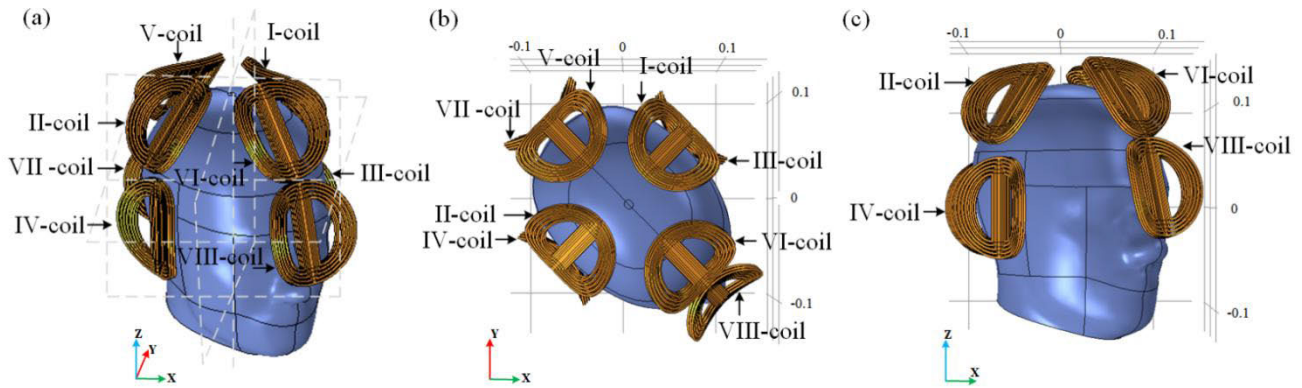
FIGURE 1. Spatial structure of the MQS array and its relative position to the human head. The solid black lines with arrows in the figure mark the position and number of each coil in the MQS array. (a) Main view of the MQS array. (b) Vertical view of the array on XY. (c) Side view of the array on XZ.
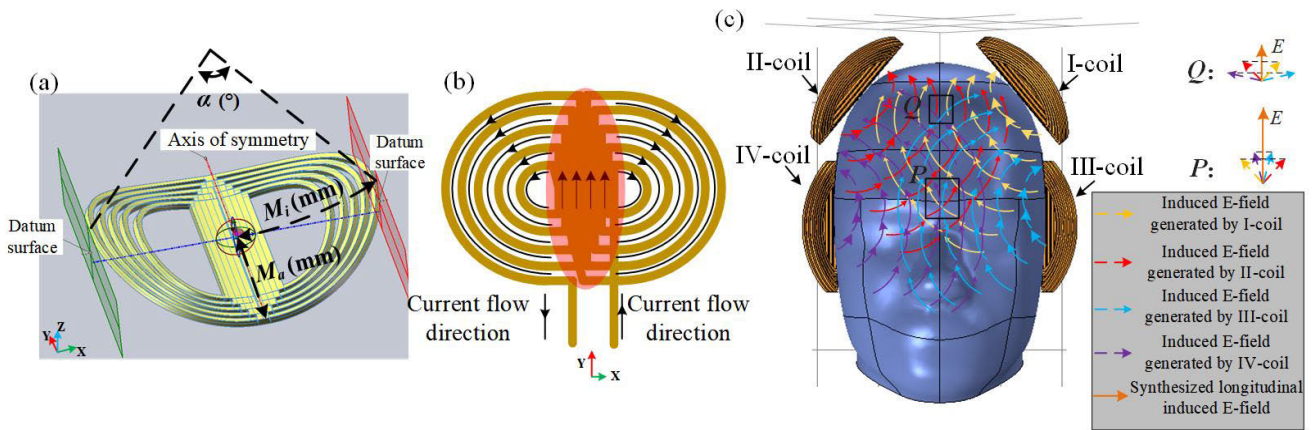
FIGURE 2. Spatial structure of the MQS array and its relative position to the human head. The solid black lines with arrows in the figure mark the position and number of each coil in the MQS array. (a) Main view of the MQS array. (b) Vertical view of the array on XY. (c) Side view of the array on XZ.

The quadrantal coils in the MQS array are divided into upper and lower layers and placed around the human head. The double-layer spatial structure of the MQS array helps ensure stimulation depth and enhances the superposition effect of the induced E-field in the deep brain.

The quadrantal coils are bent away from the human head and tangent to the scalp to fit the outline of the human head, which can reduce the accumulation of intracranial non-longitudinal induced E-field, increase the longitudinal attenuation ratio, and improve the stimulation focalization in the deep brain. The 3D geometry of the quadrantal coil is shown in Fig. 2(a).

The geometry of the coil can be described by three main parameters: the length of the semi-major axis M_a, the length of the semi-minor axis M_i, and the bending angle α. In this paper, the quadrantal coil was first modeled on the SOLIDWORKS platform and then imported to the COMSOL Multiphysics platform to complete the finite element numerical simulation. The main steps of coil modeling include sketching, plane stretching, and adding bending characteristics.

The geometric structures and current flowing directions of the quadrantal coil when projected onto the XY plane are

shown in Fig. 2(b). The red lines with arrows between the copper conductors indicate the direction of flow of the stimulation current. The current direction of the central conductors of the quadrantal coil is unified, thus the induced E-field under the central conductors of the coil can be enhanced, forming a focused stimulation area. It should be noted that in practice, the quadrantal coil is tightly wound into multi-turn and multi-layer structures, and there is no large gap between copper wires. The red transparent ellipse indicates the area where the induced E-field was strengthened below the quadrantal coil.

B. PRINCIPLE OF THE MQS ARRAY
The induced E-field distributions on the plane where the centers of I-coil to IV-coil are located are taken as an example to explain the working principle of the MQS array (Fig. 2(c)). The yellow, red, blue, and purple dotted lines with arrows stand for the induced E-field generated by the I-coil, II-coil, III-coil, and IV-coil, respectively. The arrows indicate the direction of the induced E-field, and the size of the arrows is proportional to the amplitude of the induced E-field. The four coils are symmetrical concerning the head, each at approximately equal distance from the center of the head.
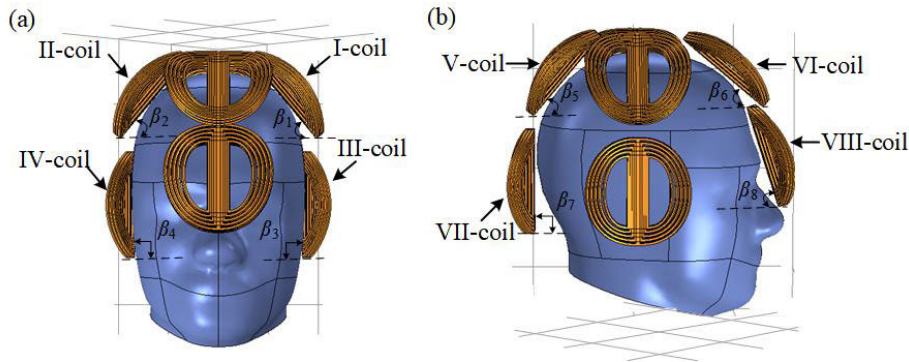
FIGURE 3. Details of the quadrantal coils' locations. The solid black lines with arrows in the figure mark the position and number of each coil in the MQS array. β presents the angle between the quadrantal coil and the XY plane. (a) The locations of I-coil, II-coil, III-coil, and IV-coil. (b) the locations of V-coil, VI-coil, VII-coil, and VIII-coil.

TABLE 1. The coordinates of each quadrantal coil in the MQS array.

Coils Coordinates	I-coil	II-coil	III-coil	IV-coil	V-coil	VI-coil	VII-coil	VIII-coil
X(cm)	5.5	-5.5	7.1	-7.1	-5.5	7.1	-8.0	9.9
Y(cm)	5.5	-5.5	7.1	-7.1	5.5	-7.1	8.0	-9.9
Z(cm)	11.0	11.0	2.0	2.0	11.0	11.0	2.0	2.8
included angle $\beta(°)$	$\beta_1=50°$	$\beta_2=50°$	$\beta_3=90°$	$\beta_4=90°$	$\beta_5=50°$	$\beta_6=50°$	$\beta_7=90°$	$\beta_8=78°$

When the stimulation currents in each quadrantal coil are equal, the amplitudes of the induced E-field vectors generate–d by the coils in the central region of the deep brain are similar and the included angles between the four induced E-field vectors are small. Accordingly, the amplitude of the synthesized longitudinal induced E-field is large (point *P*). For the stimulated points near the human scalp, the amplitude differences of the induced E-field vector generated by the four quadrantal coils are large, as are the included angles between four induced E-field vectors. Therefore, the amplitude of the synthesized longitudinal induced E-field is small in the region near the human scalp (point *Q*).

Similarly, on the plane where the center of the V-coil to VII-coil are located, the induced longitudinal E-field is also stronger in the deep brain than in the region near the scalp.

With the specific spatial structure and unique geometry, the proposed MQS array can weaken the induced E-field in the superficial region near the scalp, enhance the induced E-field in the deep brain, and generate an obvious focalized induced E-field in the deep brain. In the subsequent work, the 3D spatial distribution of the intracranial induced E-field obtained by our finite element analysis calculations also coincided with this principle. This design is advantageous for improving the stimulation effect of deep brain magnetic stimulation in multiple aspects.

III. 3D FINITE ELEMENT NUMERICAL MODEL
To analyze the distribution of the intracranial-induced E-field generated by the MQS array, numerical finite element modeling is required, mainly for the array and the stimulated head modeling.

A. THE MQS ARRAY
The geometric parameters of quadrantal coils in the array directly impact the spatial distribution of the intracranial-induced E-field. If the coil size is too large, the focusing area will be large, and when the coil size is small, it is not conducive to improving the stimulation depth. Based on previous research foundations and simulation experience, we have learned that the radius of conventional circular magnetic stimulation coils used in the human head in clinical practice is usually between 30mm and 50mm [27]. The quadrantal coil can be seen as a deformation structure of a single circular coil. Considering its applicability to the size of the human head, the length of the semi-minor axis M_i and the length of the semi-major axis M_a of the quadrantal coil are set within the radius range of the conventional circular coil: $M_a = 40mm$ and $M_i = 30mm$. After pre-calculation before simulation, we found that the small bending angle leads to less significant improvement in the focusing area. Meanwhile, as the bending

angle increases, the stress borne by the coil skeleton and copper wire in the actual processing process will continue to increase. Considering the improved effect on stimulation focalization and the practical engineering requirements in subsequent experiments, the bending angle α is set at 80° in our manuscript.

The total number of turns of the quadrantal coil is 16 and the number of layers is 4. The conductivity of the copper wire is 5.998×10^7 S/m and the size of the copper wire was 3 mm×4 mm. Considering the obstacles of hair and coil packaging in practice, the distance between the quadrantal coil and the human scalp was set to 5 mm.

The locations of the quadrantal coils are shown in Fig.3. The coordinates of each quadrantal coil's center point and the angle β between the quadrantal coil and XOY plane are listed in Table. 1.

B. THE HUMAN HEAD

An anatomically realistic human head model, which comes from the Population Head Model (PHM) repository, is employed in this study to verify our method. The PHM repository was developed by Lee using the SimNIBS pipeline, which was utilized to segment anatomical regions from Human Connectome Project MRI images [28]. The biological conductivity of the gray matter is set at 1.07×10^{-1} S/m [29]. The center point of the human head model was set as the origin of the space coordinate system, and the coordinates of the scalp vertex are $X = 0$, $Y = 0$, and $Z = 12.4$ cm.

C. MESHES

The human head model and the proposed MQS array model were imported to the COMSOL Multiphysics platform, and the finite-element (FE) method was adopted to calculate the spatial distribution of the intracranial E-field generated by the MQS array. To disregard mesh differences when comparing the influences of different stimulation currents, all FE models had the same mesh size and were computed twice.

The details of the mesh size in this study are as follows: the maximum element size is 0.0066 m, the maximum element growth is 1.4 and the curvature factor is 0.4. Because our major concern is the spatial distribution of the induced E-field in the deep brain, the gray matter is meshed finer, the minimum element size for the gray matter is 0.001m and for the rest parts of the FE model, the minimum element size is set at 0.002. The grid level is sufficiently fine, and the computation converges smoothly.

IV. MULTI-OBJECTIVE OPTIMIZATION OF THE MQS ARRAY
A. DEFINITIONS OF IMPORTANT INDUCED E-FIELD CHARACTERISTICS IN DEEP BRAIN

The targeted tissues in many mental disorders are not superficial. Considering the depth requirement of deep brain

transcranial magnetic stimulation, the stimulation depth is set at 10cm below the scalp.
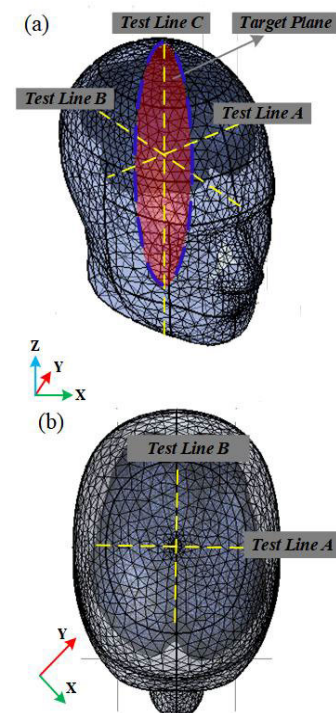
To analyze the 3D distributions of the induced E-field generated by the MQS array in the deep brain, three intracranial test lines (*Test Line A*($X = Y$, $Z = 2.4$ cm), *Test Line B* ($X = -Y$, $Z = 2.4$ cm), *Test Line C* ($X = Y = 0$)), and one longitudinal *Target Plane* was set as in Fig. 4.

The definitions of the objectives that need to be optimized in this study are as follows:

(1) *Intensity*: Under identical stimulation current, a higher amplitude of the induced E-field means stronger stimulation and it is more possible to change the membrane potential of nerve cells. The E_{max} was measured on Test Line A and Test Line B to characterize the stimulation intensity [30].

(2) *Focalization*: S_{70} was adopted to evaluate the stimulation focalization from the 2D level. S_{70} represents the focusing area on the target plane where the amplitude of the induced E-field exceeds $E_{max} / \sqrt{2}$ [31], [32], [25]. The smaller the S_{70}, the fewer un-targeted tissues are under strong stimulation, the fewer un-targeted tissues are under strong stimulation, and the better the stimulation focalization. The value of S_{70} was calculated on the longitudinal *Target Plane*.

(3) *Intracranial longitudinal attenuation ratio*: The attenuation feature of the induced E-field was evaluated using the ratio $\delta = E_{6cm} / E_{2cm}$ [21], [22], [25]. E_{2cm} and E_{6cm} are the intensities of the E-field at stimulation depths of 2cm and 6cm below the human scalp, respectively. The larger the ratio

FIGURE 4. The meshed 3D model of the human head. Three intracranial test lines Test Line A (X = Y, Z = 2.4 cm), Test Line B (X = - Y, Z =2.4 cm), Test Line C (X = Y =0)), and one longitudinal Target Plane are marked in the figure.
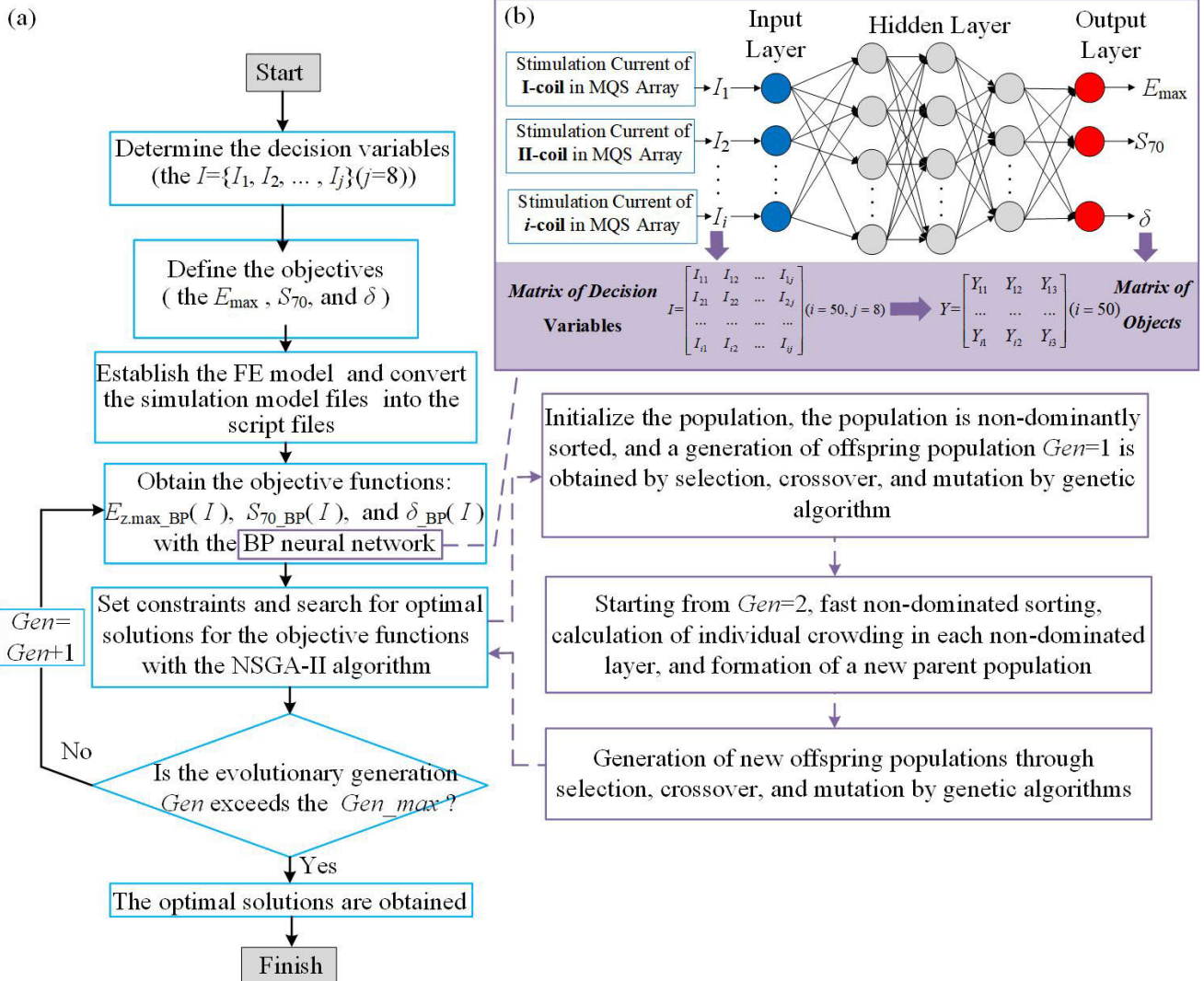
(a)

(b)

FIGURE 5. Flow chart of the proposed BP-NSGA-II algorithm optimization method. (b) The structure of the MQS array predictive models based on the BP neural network.

δ means that when the intensity of the induced E-field in the deep brain remains unchanged, a weaker induced E-field will remain in the superficial region, and the better the attenuated performance of the intracranial induced E-field. Unlike the skull, the human scalp has pain sensation nerves, so the stronger the stimulation intensity in the superficial region, the more likely it is to cause pain, which also means the larger the ratio δ, the less pain. The intracranial longitudinal attenuation δ was measured along *Test Line C*.

B. THE BP-NSGA-II ALGORITHM OPTIMIZATION METHOD

When the geometry of the stimulation array and its relative position to the human head is determined, the spatial distributions of the intracranial induced E-field generated are determined by the stimulation current configuration.

In this paper, the pulse width of the stimulation current is set at 200 μs and the amplitudes of the stimulation current

applied in I-coil to VIII-coil are expressed as I_1, I_2, I_3, I_4, I_5, I_6, I_7, and I_8, respectively. Hence, the decision variables in the optimization can be defined as $I=\{I_1, I_2, \ldots, I_j\}$. j is the number of coils in the array to be optimized and in this study $j = 8$.

There are three important characteristics: stimulation intensity E_{max}, focalization S_{70}, and longitudinal attenuation ratio δ of the intracranial induced E-field that need to be discussed when evaluating the deep brain transcranial magnetic stimulation performance of TMS arrays. To optimize the stimulation effect of the MQS array from multiple perspectives, E_{max}, S_{70}, and δ were chosen as the optimization objectives in this paper. However, the three optimization objectives may conflict with each other. The improvement of one objective may result in the degradation of the other objective's performance. Multi-objective optimization methods are often used to solve the problem of several nonlinear

objectives in the same model, and multiple conflicting objectives must be optimized simultaneously [33].

There are two major difficulties in the multi-objective optimization of the TMS array: one is that the explicit analytic relationships between the stimulation currents (the decision variables) and the characteristics of the induced E-field generated by the MQS array (the objectives) are hard to obtain directly through mathematical derivation. Another difficulty is that not only do they have multiple conflict objectives, but there are also multiple independent decision variables, which makes the optimization process more complex.

To solve these problems, choosing appropriate algorithms is crucial. As a multi-objective optimization algorithm, the NSGA-II algorithm has the advantages of fast convergence, diversity maintenance, and high adjustability. These advantages are beneficial and suitable for solving problems involving multiple nonlinear objectives and conflicting objectives in the optimization process of MQS arrays. Accordingly, the NSGA-II algorithm is used to realize the multi-objective optimization of the MQS array. The BP neural network algorithm is an intelligent algorithm that simulates the biological organization of the human brain and has the advantages of a simple model and low computational effort. It can solve the problem of the limited ability to fit explicit functions by learning various training sets to fit the intrinsic relationship between the decision variables and the objective function. It also has the advantage of strong nonlinear mapping ability and is good at solving problems with complex internal mechanisms that are suitable for establishing relationships between stimulation currents and the characteristics of the induced E-field generated by the MQS array. Based on these advantages, the BP neural network algorithm is adopted in this study to acquire the objective functions that reflect the mapping relationships between the conflicting objectives and the decision variables.

As the field of algorithms continues to evolve, it is expected that the optimization speed, as well as the prediction accuracy, will be further improved in the future if algorithms more suitable for solving the magnetic stimulus array optimization problem emerge. It should be noted that with the development of the algorithms, the magnetic array optimization method mentioned in this manuscript which combines the predictive model with the multi-objective optimization algorithm will still be applicable.

The proposed BP-NSGA-II algorithm optimization method is shown in the block diagram in Fig.5. Its major steps are concluded as follows:

Step①: Determine the decision variables ($I = \{I_1, I_2, \ldots, I_j\}, j = 8$).

Step②: Define the objectives (E_{max}, S_{70}, and δ).

Step③: Establish the FE model of the MPS array and the human head, and convert the simulation model files (.*mph file*) of the COMSOL Multiphysics platform into the script files (.*m file*) that can be recognized and run on MATLAB.

Step④: The initial values of $i = 50$ sets of stimulation currents are obtained with the Latin hypercube function and

assigned to the MQS array for FEM calculation. The matrix of decision variables I is shown in Equation .1. The matrix of objects Y is shown in Equation.2.

I_{ij} means the amplitude of the stimulation current of the j-coil in the i-th set of stimulation currents. Y_{i1}, Y_{i2}, and Y_{i_3} stand for the stimulation intensity E_{max}, S_{70}, and δ generated by the i-th set of stimulation.

$$
I = \begin{bmatrix} I_{11} & I_{12} & \ldots & I_{1j} \\ I_{21} & I_{22} & \ldots & I_{2j} \\ \ldots & \ldots & \ldots & \ldots \\ I_{i1} & I_{i2} & \ldots & I_{ij} \end{bmatrix} (i = 50, j = 8) \quad (1)
$$

$$
Y = \begin{bmatrix} Y_{11} & Y_{12} & Y_{13} \\ \ldots & \ldots & \ldots \\ Y_{i1} & Y_{i2} & Y_{i3} \end{bmatrix} (i = 50) \quad (2)
$$

The 50 sets of simulation data are used to train and test the BP neural network. The predictive models obtained based on the BP neural network are used as the objective functions in the following multi-optimization.

Step⑤: Set constraints and search for optimal solutions for the objective functions with the NSGA-II algorithm.

The irregular structures of the human head and the MQS array make the FE numerical simulation models complex. Discontinuities in electrical conductivity and magnetic permeability of biological brain tissues increase the amount of calculation for the FE numerical simulation. If the FE simulation numerical calculation platform is used directly for both analysis and optimization, repeated iterative cycles are required to solve the new iterative equations, which leads to high time costs and difficulty in realizing multi-objective optimization. Therefore, the co-simulation method of COMSOL Multiphysics and MATLAB Livelink is used in this study to perform the BP-NSGA-II algorithm optimization method and search for the optimal configuration of the stimulation current of the MQS array.

C. PREDICTIVE MODELS OBTAINED WITH BP NEURAL NETWORK ALGORITHM

As an intelligent algorithm, the BP neural network is a multi-layer feed-forward network trained according to the error backpropagation algorithm, which consists of three parts: the input layer, hidden layer, and output layer. The basic idea is to realize gradient descent, which uses error backpropagation and iterative learning training to minimize the error between the actual output value and the desired output value of the network.

The structure of the MQS array predictive models based on the BP neural network is shown in Fig. 5(b). The input variables in the prediction models were the stimulation currents $I = \{I_1, I_2, \ldots, I_8\}$. The predictive models built for E_{max}, S_{70}, and δ are denoted as $E_{max\_BP}(I)$, $S_{70\_BP}(I)$, and $\delta_{\_BP}(I)$, respectively.

The initial values of $i = 50$ sets of stimulation currents I in the range of {1kA, 5kA} were obtained using the Latin hypercube function. Each set of stimulation currents was assigned to the MQS array to obtain the spatial distribution

characteristics of the generated induced E-field. Based on the 50 sets of data, the BP neural network was used to establish the predictive models that reflect the mathematical mapping relationships between the stimulation currents $I = \{I_1, I_2, \ldots, I_8\}$ and the characteristics of the induced E-field generated by the MQS array.

Key parameters in the BP neural network algorithm: training times *net.trainParam.epochs* = 1000, learning rate *net.trainParam.lr* = 0.01, minimum error of training target *net.trainParam.goal* = 0.000001. Among the 50 sets of data, *TrainN* groups of them are used for training data, and *TestN* groups of them are used for testing data. The sum of *TrainN* and *TestN* was fixed at $i = TrainN + TestN = 50$.

When *TrainN*=45, the rest 5 groups of data were used to test the accuracy of the BP neural network, and a comparison between the predicted values and expected values of the BP neural network test set is shown in Fig.6. The correlation

coefficient R^2 between the predicted and expected values of the BP neural network is $R^2 > 95\%$ which reached a significant level, proving the reliability of the BP neural network predictive models $E_{\max\_BP}(I)$, $S_{70\_BP}(I)$, and $\delta\_{BP}(I)$.

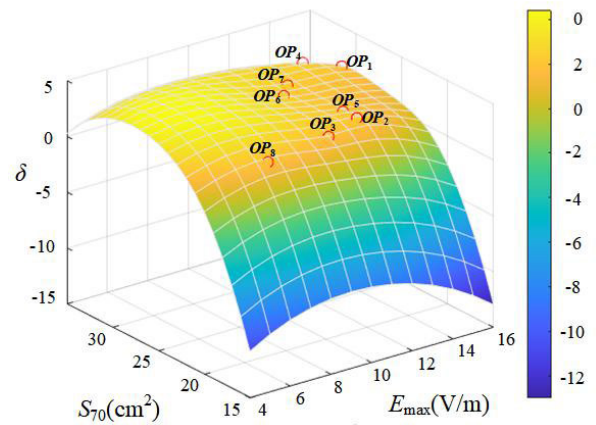### D. MULTI-OBJECTIVE OPTIMIZATION OF ARRAY STIMULATION CURRENTS

NSGA - II is one of the most popular multi-objective genetic algorithms, and it uses a fast non-dominated sorting algorithm. Its computational complexity is significantly reduced compared to that of NSGA. An elite strategy is also introduced to expand the sampling space, prevent the loss of the best individual, and improve the operation speed and robustness of the algorithm. The multi-objective function and constraint in this study are defined as follows:

$$\begin{cases} Max\left(E_{\max\_BP}(I)\right) \\ Min\left(S_{70\_BP}(I)\right) \\ Max\left(\delta\_{BP}(I)\right) \\ 1\,kA \le I = \{I_1, \quad I_2, \ldots, \quad I_8\} \le 5\,kA \end{cases} \quad (3)$$

Key parameters in the NSGA - II algorithm: fitness function deviation *TolFun*=1e-10, size of the population *populationsize*=40, and the maximum evolutionary generation *Gen_max*=50. There are eight optimal solutions in the obtained Pareto set. The Pareto front is shown in Fig. 7, the red points OP_1-OP_8 indicate the value of the multi-objective function corresponding to each solution in the Pareto set.
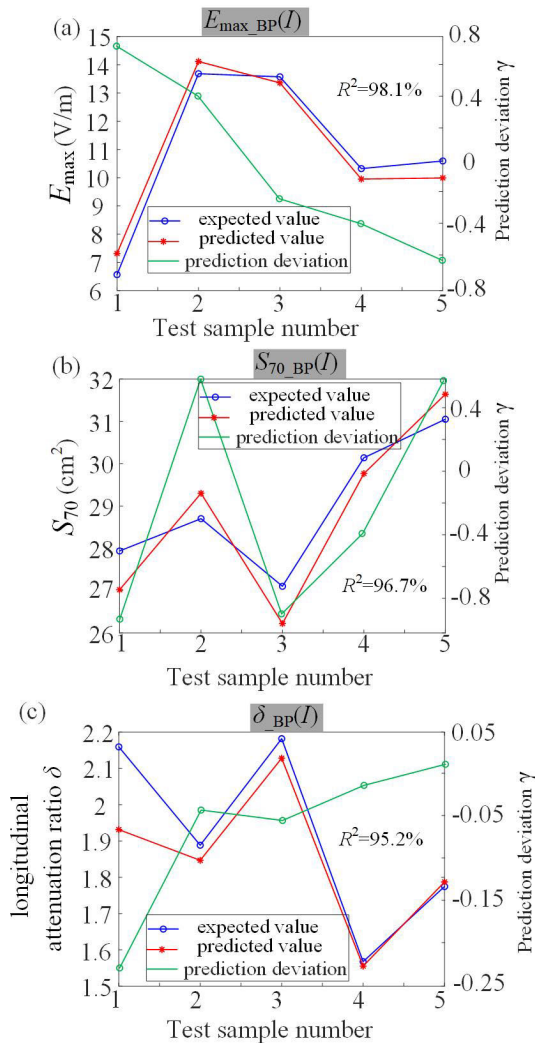
FIGURE 6. Comparisons between the predicted values and expected values of the BP neural network when *TrainN* =45. (a) The predictive model $E_{\max\_BP}(I)$. (b) The predictive model $S_{70\_BP}(I)$. (c) The predictive model $\delta\_{BP}(I)$.

FIGURE 7. Pareto front obtained with multi-objective optimization. The hollow circles OP_1-OP_8 indicate the value of the multi-objective function corresponding to each solution in the Pareto set.

The values of the decision variables $I = \{I_1, I_2, \ldots, I_8\}$ corresponding to each optimal solution were imported into the COMSOL model for finite element numerical calculation. Comparing the results obtained with the FE numerical analysis with those obtained from the NSGA-II algorithm (Table.2), the average error Δ between the values obtained from the FE numerical calculation and the predict–ive values of the algorithm are less than 8%, which in turn proves that the BP prediction model is reliable.

TABLE 2. Comparison of the results obtained by FE numerical analysis with those obtained by BP-NSGA-II algorithm.

Pareto frontier solutions	Decision variables $I=\{I_1,I_2,I_3,I_4,I_5,I_6,I_7,I_8\}$ (kA)	Predicted value with BP-NSGA-II algorithm			Expected value with FE numerical calculation			Average error
		E_{max} (V/m)	S_{70} (cm^2)	δ	E_{max} (V/m)	S_{70} (cm^2)	δ	$\varDelta$
OP_1	{4.22,3.54,4.35,3.43,1.45,3.55, 1.65, 2.22}	15.00	30.94	1.82	13.00	30.00	1.80	6.3%
OP_2	{2.03,2.44,4.24,4.54,1.38,3.59, 1.71,2.46}	12.70	23.00	2.22	12.40	26.01	2.25	5.1%
OP_3	{4.63,2.19,2.31,3.96,1.21,2.63, 1.16,2.32}	11.00	21.94	1.79	11.00	25.25	1.74	5.3%
OP_4	{2.59,3.19,4.73,4.46,1.46,3.49, 1.43,2.46}	14.43	32.38	2.17	13.90	28.00	2.10	7.7%
OP_5	{2.03,2.43,4.77,4.57,1.44,3.58, 1.73,2.44}	12.90	24.48	2.00	13.30	26.08	2.30	7.3%
OP_6	{2.03,2.43,4.28,4.54,1.42,3.59, 1.73,2.45}	11.66	28.29	2.38	12.05	27.00	2.37	2.9%
OP_7	{2.03,2.43,4.31,4.55,1.39,3.59, 1.73,2.46}	12.50	29.77	2.27	12.58	26.90	2.28	4.0%
OP_8	{2.07,2.72,2.61,3.20,1.01,2.66, 1.70,4.96}	7.50	21.00	1.89	7.00	23.35	1.83	6.8%

Among the three characteristics, the maximum error comes from the data of the stimulation focalization S_{70}. This is because the stimulation intensity E_{max} is a maximum value and it can be calculated at a specific probe point on the test line. The intracranial longitudinal attenuation ratio δ is the ratio of the induced E-field strength at the two specific probe points. However, the focusing area is composed of innumerable data points on the target plane where the induced E-field is greater than a specific threshold. The integral-derived value calculation method was used to calculate the area of the irregular region formed by the data points, which leads to a greater error in the calculation of S_{70} than that of E_{max} and δ.

As we can see from the eight optimal solutions: the strongest stimulation intensity $E_{max} = 13.9$ V/m is obtained at OP_4; the smallest focusing area $S_{70} = 23.35$ cm^2 is obtained at OP_8; the best longitudinal attenuation $\delta = 2.37$ is obtained at OP_6. It needs to be explained here that considering the higher requirements for stimulation intensity in clinical applications, the stimulation intensity can be further enhanced by increasing the amplitude range of the stimulation current in the constraint conditions or increasing the total number of coil turns.

V. COMPARISON AND DISCUSSION

A. CONSTRAINTS
The geometric structure of the TMS array and the stimulation currents applied in the array not only affect the spatial distribution of the intracranial induced E-field but also influence the Joule power loss. To enrich comparison, two traditional planar coil arrays are employed in this study as the reference group for comparison with the optimized MQS array.

According to the law of resistance, the resistance of the unit coil element can be expressed as:

$$dR = \rho \frac{2\pi R_0}{dS} \qquad (4)$$

where R_0, ρ, and dS represent the radius, copper wire resistivity, and cross-sectional area of one unit coil element, respectively.

When the current density of the stimulating current applied to the copper wire is $j_{current}$, the Joule power per unit coil element is:

$$dP = (j_{current}\, dS)^2 dR \qquad (5)$$

Substituting Equation 4 into Equation 5 yields:

$$dP = j^2_{current}\rho \times 2\pi R_0 \times dS = j^2\rho \times dV \qquad (6)$$

where dV is the volume per coil element, and the power consumption of the entire coil should be the integral of dP to the entire conductor volume.

Therefore, according to the geometric structure of a circular coil, the coil power loss of a single circular coil can be expressed as:

$$P_{SC} = j^2_{current}\rho \times 2b(R_1^2 - R_0^2)\pi \qquad (7)$$

where the inner diameter of the single circular coil is R_0, the outer diameter is R_1 and the height is b. If eight single circular coils of identical geometry form a conventional stimulated array, the total Joule power of the single circular coil array is:

$$P_{\text{SC-array}} = \sum_{m=1}^{8} j_{current\_m}^2 \times \rho \times 2b(R_1^2 - R_0^2)\pi \quad (8)$$

In this study, eight geometrically identical single circular coils with an inner diameter of R_0 =15mm, outer diameter of R_1 =35mm, and height of $b = 16$mm were used to form the conventional planar single circular array (the SC array). The layout of the single-layer SC array is 2×4 and the layout of the double-layer array is 2×2.

The Joule power loss of the MQS array and the SC array after one pulse is W_0 and $W_{SC-array}$, respectively. The constraint is defined as:

$$W_0 = W_{SC-array} = P_{\text{SC\_array}} \times t \quad (9)$$

Assuming that the stimulation current amplitudes applied to each circular coil of the reference array are equal to $j_{current\_0}$, the optimized MQS array at OP_5 was taken as the experimental array. When the decision variables $I(kA)=\{I_1, I_2, \ldots, I_8\}=\{2.03,2.43,4.77,4.57,1.44,3.58,1.73,2.44\}$, the Joule power of the MQS array is W_0 =60J, which gives $j_{current\_0}$ =55.8 A/cm^2 in the reference array. Based on our calculation, under this current configuration, the maximum stress and temperature rise of the stimulating coil is less than 12 Mpa and 0.1°/pulse, respectively. And it is indicated to be a safe value as in [34] and [35].

B. COMPARISON OF THE INTRACRANIAL INDUCED E-FIELDS BETWEEN THE OPTIMIZED MQS ARRAY AND THE REFERENCE ARRAY

At a current density of $j_{current\_0}$ =55.8 A/cm^2, the stimulation intensity, focusing area, and longitudinal attenuation ratio of the intracranial induced E-field generated by the conventional single-layer SC array and double-layer SC array at the same stimulation depth with the MQS array are fully calculated as in Table.3.

TABLE 3. Data comparison of three different arrays.

Coil arrays	E_{max} (V/m)	S_{70} (cm^2)	δ
the optimized MQS array	13.30	26.08	2.30
the single-layer SC array	5.75	110	0.51
the double-layer SC array	7.08	110.2	0.455

The distribution of the intracranial induced E-field generated by the conventional SC arrays and optimized MQS arrays along *Test Line C* is shown in Fig.8. The optimized

MQS array produces a significant peak value in the deep intracranial region, whereas the induced E-field generated by the conventional planar SC array decays rapidly with an increase in stimulation depth, and no significant focusing area is generated in the deep brain. Comparing the solid green line with the solid orange line in Fig. 8, it can be seen that the optimized MQS array can enhance the stimulation intensity in the deep brain by 131% and increase the longitudinal decay ratio to 4.5 times compared with the conventional planar single-layer SC array with the same Joule loss.
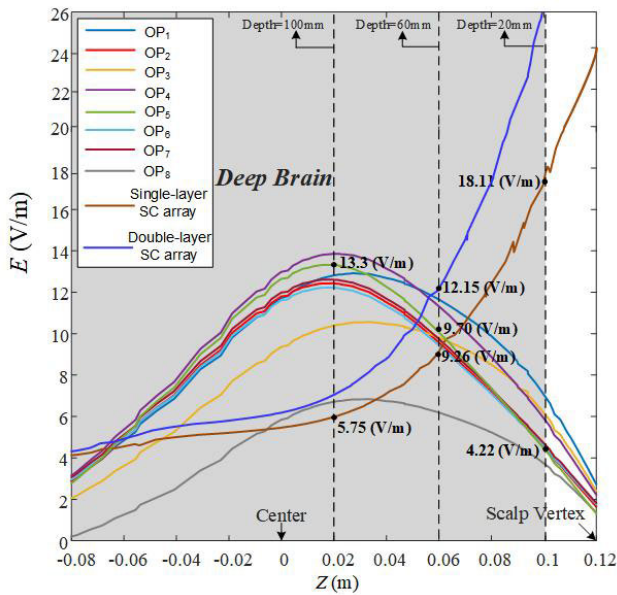
The spatial distributions of the induced E-field generated by the conventional SC arrays and optimized MQS array on the intracranial longitudinal target plane are shown in Fig. 9. The optimized MQS array can produce a significant focusing area in the deep brain, whereas the induced E-field generated by the SC array is concentrated in the superficial region. The focusing area generated by the conventional single-layer SC array at the stimulation depth of 10 cm is 110 cm^2, which means at the same Joule loss, the optimized MQS array reduces the focusing area in the deep brain region by 76% compared to the conventional planar single-layer SC array.

After satisfying the therapeutic demands, the practical possibility of realizing the MQS array is considered and discussed based on our previous experience in developing coils and the advanced coil manufacturing technology in the State Key Laboratory of Advanced Electromagnetic Engineering and Technology, Wuhan Nation High Magnetic Field Center (WHMFC) [34], [36], [37]. The quadrantal coil in this paper can be wound by copper wires with a cross-section of 3mm×4mm and conductivity of 5.998×10^7S/m. It can be supported by a special-shaped framework processed with an epoxy featuring high strength and high corrosion resistance properties.

The outermost layer of the coil can also be reinforced with epoxy. Then the MQS array can be built by placing the eight coils at certain positions around the human head with the help of the fixing bracket.

VI. FURTHER WORK

Achieving a satisfied deep brain transcranial magnetic stimulation effect is very difficult. However, since many important stimulated targets are located far away from the scalp, using non-invasive or invasive methods to achieve good deep brain transcranial magnetic stimulation effects is an unavoidable issue for both clinical applications and scientific research. Before applying our design to biological experiments involving small rodents and humans, it is necessary to strictly debug the prototype equipment and complete a series of biological experiment safety tests. In future studies, we will build an experimental platform based on our experience in developing pulse power supplies and magnetic coils in WHMFC, and collaborate with the hospital (Clinical Hospital of Chengdu Brain Science Institute, MOE Key Lab for Neuroinformation) where the author works to gradually carry out follow-up

FIGURE 8. Comparisons of the intracranial induced E-field distributions along Test Line C generated by the conventional single-layer SC array, double-layer SC array, and optimized MQS arrays. The light gray part means the deep brain regions where the is deeper than 20mm below the scalp.

work. During the experimental validation stage, the following three main issues need to be addressed:

(1) Processing and fabrication of the optimized array. The processing process of the quadrantal coil is similar to conventional coils, but due to the special curved structure, the coil winding skeleton and the array support bracket need to be designed and processed separately. We have discussed with WHMFC and are ready to process the coil skeleton with the help of 3D printing technology. The coil skeleton material is planned to be made of photosensitive resin liquid material, and the array's support bracket is designed with epoxy resin.

(2) Set up the multi-channel stimulation system. For the eight-channel array in this paper, the modular power supply driver circuit should be further designed to provide stimulation currents for the array. A specific control module should be considered to realize the function of online optimization and flexible adjustment of array stimulation parameters.

(3) Construction of a head mimic. To extract the spatial distributions of the induced E-field in the human head, we need an experimental model of the head mimic. Combined with medical measurement data, the biological tissues within the human head are simulated using specific physiological solutions with close electromagnetic parameters. For example, the cortical tissue mimetic solution can be made by mixing 40% sugar solution and 0.02% potassium chloride powder.

(4) When the experimental platform and test system commissioning are completed, we will use the research platform of the School of Life Sciences at the University of Science and Technology of China to conduct animal experiments with
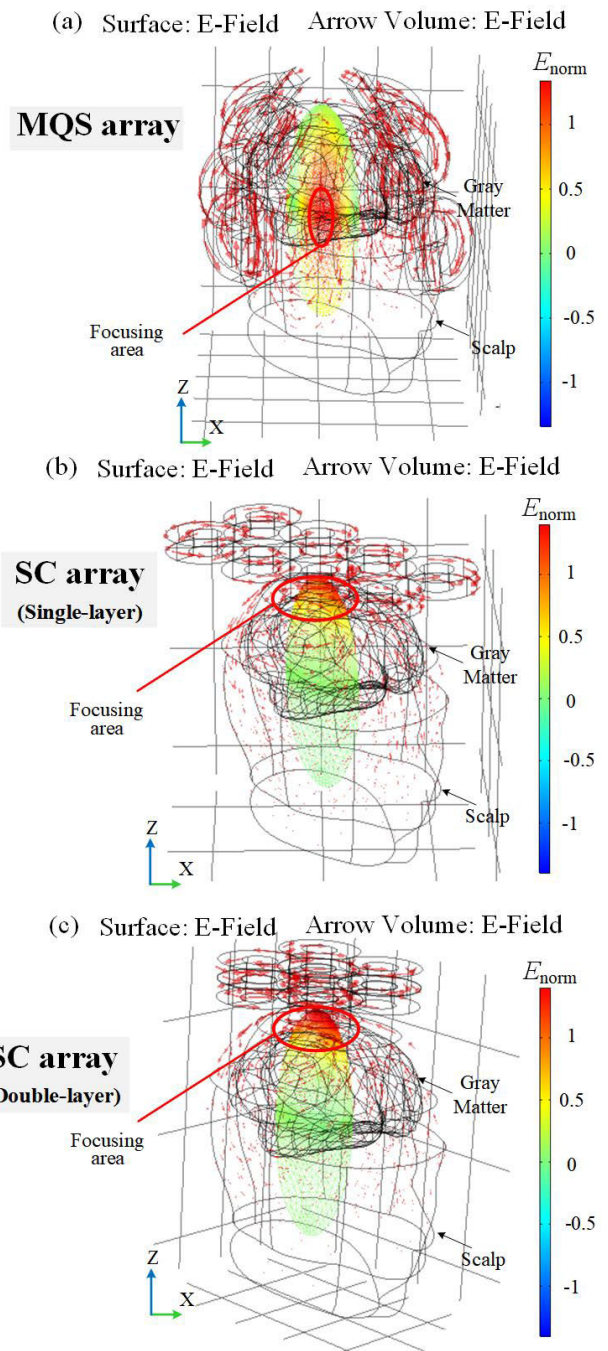
FIGURE 9. The spatial distributions of the induced E-field generated by the conventional single-layer SC array, double-layer SC array, and optimized MQS array (at OP_5) on the intracranial longitudinal target plane.

small rodents or humans, and further psychiatry validation of the effects of deep brain transcranial magnetic stimulation.

VII. CONCLUSION
In this study, we introduce the MQS array to improve the stimulation effect of TMS in the deep brain. Due to the geometric bending characteristics of quadrant coils and their unique relative position with the human, the accumulation

of non-longitudinal components of the intracranial induced E-field can be reduced and the stimulation focalization can be improved. The double-layer structure of the MQS array is conducive to enhancing the superposition effect of the intracranial-induced E-field in the deep brain region, increasing the stimulation depth as well as the longitudinal attenuation ratio. Based on the geometric design of the MQS array, the BP-NSGA-II algorithm optimization method is proposed to further improve the stimulation effect in the deep brain. The BP neural network algorithm is used to obtain the predictive models of the MQS array and then the NSGA-II algorithm is adopted to optimize the stimulation currents in the MQS array with multiple objectives. Results showed that the MQS array proposed in this paper could produce an obvious focusing area 10 cm below the scalp and improve the deep brain transcranial magnetic stimulation effect in several aspects. Under the same Joule loss, the optimized MQS array can increase the stimulation intensity by 131%, reduce the focusing area by 76%, increase the longitudinal attenuation ratio to 4.5 times, and significantly optimize the 3D distributions of the intracranial induced E-field in the deep brain compared with the conventional planar TMS array. The proposed optimization method can also be well applied to the optimization process of coils or arrays in other application contexts. The focus of this paper is to present the geometric design of the MQS array and its optimization method. Achieving focalized stimulation in the deep brain is an important research direction for TMS, and we hope that the work in this paper can provide new ideas for improving the deep brain transcranial magnetic stimulation effects and lay the foundation for further broadening the application of TMS.

REFERENCES

[1] K. A. Sathi, Md. A. Hossain, M. K. Hosain, N. H. Hai, and M. A. Hossain, "A deep neural network model for predicting electric fields induced by transcranial magnetic stimulation coil," *IEEE Access*, vol. 9, pp. 128381–128392, 2021, doi: 10.1109/ACCESS.2021.3112612.

[2] M. C. Gomez-Alvaro, S. Villafaina, J. L. Leon-Llamas, A. Murillo-Garcia, M. Melo-Alonso, J. Sánchez-Gómez, P. Molero, R. Cano-Plasencia, and N. Gusi, "Effects of transcranial direct current stimulation on brain electrical activity, heart rate variability, and dual-task performance in healthy and fibromyalgia women: A study protocol," *Behav. Sci.*, vol. 12, no. 2, p. 37, Feb. 2022.

[3] A. Aleman, "Use of repetitive transcranial magnetic stimulation for treatment in psychiatry," *Clin. Psychopharmacology Neurosci.*, vol. 11, no. 2, pp. 53–59, Aug. 2013.

[4] J. Liepert, S. Zittel, and C. Weiller, "Improvement of dexterity by single session low-frequency repetitive transcranial magnetic stimulation over the contralesional motor cortex in acute stroke: A double-blind placebo-controlled crossover trial," *Restorative Neurol. Neurosci.*, vol. 25, pp. 5–6, Jun. 2007.

[5] O. F. Afuwape, P. Rastogi, and D. C. Jiles, "Comparison of the effect of coil configuration and the variability of anatomical structure on transcranial magnetic stimulation," *IEEE Trans. Magn.*, vol. 57, no. 2, pp. 1–5, Feb. 2021.

[6] M. Lu and S. Ueno, "Comparison of the induced fields using different coil configurations during deep transcranial magnetic stimulation," *PLoS ONE*, vol. 12, no. 6, Jun. 2017, Art. no. e0178422.

[7] T. Pashut, S. Wolfus, A. Friedman, M. Lavidor, I. Bar-Gad, Y. Yeshurun, and A. Korngreen, "Mechanisms of magnetic stimulation of central nervous system neurons," *PLoS Comput. Biol.*, vol. 7, no. 3, Mar. 2011, Art. no. e1002022.

[8] M. Iwahashi, Y. Katayama, S. Ueno, and K. Iramina, "Effect of transcranial magnetic stimulation on P300 of event-related potential," in *Proc. Annu. Int. Conf. IEEE Eng. Med. Biol. Soc.*, Sep. 2009, pp. 1359–1362.

[9] N. Attal, F. Poindessous-Jazat, E. De Chauvigny, C. Quesada, A. Mhalla, S. S. Ayache, C. Fermanian, J. Nizard, R. Peyron, J.-P. Lefaucheur, and D. Bouhassira, "Repetitive transcranial magnetic stimulation for neuropathic pain: A randomized multicentre sham-controlled trial," *Brain*, vol. 144, no. 11, pp. 3328–3339, Dec. 2021.

[10] Y. Noda, "Potential neurophysiological mechanisms of 1Hz-TMS to the right prefrontal cortex for depression: An exploratory TMS-EEG study in healthy participants," *J. Personalized Med.*, vol. 11, no. 2, p. 68, Jan. 2021.

[11] C. Liu, H. Ding, X. Fang, and Z. Wang, "Optimal design of transcranial magnetic stimulation thin core coil with trade-off between stimulation effect and heat energy," *IEEE Trans. Appl. Supercond.*, vol. 30, no. 4, pp. 1–6, Jun. 2020.

[12] J. Trung, A. Hanganu, S. Jobert, C. Degroot, B. Mejia-Constain, M. Kibreab, M.-A. Bruneau, A.-L. Lafontaine, A. Strafella, and O. Monchi, "Transcranial magnetic stimulation improves cognition over time in Parkinson's disease," *Parkinsonism Rel. Disorders*, vol. 66, pp. 3–8, Sep. 2019.

[13] F. Leblhuber, S. Geisler, D. Ehrlich, K. Steiner, G. Reibnegger, D. Fuchs, and K. Kurz, "Repetitive transcranial magnetic stimulation in the treatment of resistant depression: Changes of specific neurotransmitter precursor amino acids," *J. Neural Transmiss.*, vol. 128, no. 8, pp. 1225–1231, Aug. 2021.

[14] R. Chen, D. C. Spencer, J. Weston, and S. J. Nolan, "Transcranial magnetic stimulation for the treatment of epilepsy," *Cochrane Database Systematic Rev.*, vol. 8, Aug. 2016, Art. no. CD011025.

[15] S. Ueno, T. Tashiro, and K. Harada, "Localized stimulation of neural tissues in the brain by means of a paired configuration of time-varying magnetic fields," *J. Appl. Phys.*, vol. 64, no. 10, pp. 5862–5864, Nov. 1988.

[16] M. Gross, L. Nakamura, A. Pascual-Leone, and F. Fregni, "Has repetitive transcranial magnetic stimulation (rTMS) treatment for depression improved? A systematic review and meta-analysis comparing the recent vs. The earlier rTMS studies," *Acta Psychiatrica Scandinavica*, vol. 116, no. 3, pp. 165–173, Sep. 2007.

[17] S. C. P. Sousa, J. Almeida, P. C. Miranda, R. Salvador, J. Silvestre, H. Simoes, and P. Crespo, "Optimization of multiple coils immersed in a conducting liquid for half-hemisphere or whole-brain deep transcranial magnetic stimulation: A simulation study," in *Proc. 36th Annu. Int. Conf. IEEE Eng. Med. Biol. Soc.*, 2014, pp. 1–10.

[18] E. R. Lontis, M. Voigt, and J. J. Struijk, "Focality assessment in transcranial magnetic stimulation with double and cone coils," *J. Clin. Neurophysiology*, vol. 23, no. 5, pp. 463–472, Oct. 2006.

[19] Y. Roth, A. Zangen, and M. Hallett, "A coil design for transcranial magnetic stimulation of deep brain regions," *J. Clin. Neurophysiology*, vol. 19, no. 4, pp. 361–370, Aug. 2002.

[20] A. Zangen, Y. Roth, B. Voller, and M. Hallett, "Transcranial magnetic stimulation of deep brain regions: Evidence for efficacy of the H-coil," *Clin. Neurophysiol.*, vol. 116, no. 4, pp. 775–779, Apr. 2005.

[21] E. V. Harel, A. Zangen, Y. Roth, I. Reti, Y. Braw, and Y. Levkovitz, "H-coil repetitive transcranial magnetic stimulation for the treatment of bipolar depression: An add-on, safety and feasibility study," *World J. Biol. Psychiatry*, vol. 12, no. 2, pp. 119–126, Mar. 2011.

[22] V. Guadagnin, M. Parazzini, S. Fiocchi, I. Liorni, and P. Ravazzani, "Deep transcranial magnetic stimulation: Modeling of different coil configurations," *IEEE Trans. Biomed. Eng.*, vol. 63, no. 7, pp. 1543–1550, Jul. 2016.

[23] B. Lonergan, E. Nguyen, C. Lembo, C. Hinchman, O. G. Morales, D. Z. Press, A. Pascual-Leone, and A. P. Stern, "Patient- and technician-oriented attitudes toward transcranial magnetic stimulation devices," *J. Neuropsychiatry Clin. Neurosciences*, vol. 30, no. 3, pp. 242–245, Jul. 2018.

[24] S. Zibman, G. S. Pell, N. Barnea-Ygael, Y. Roth, and A. Zangen, "Application of transcranial magnetic stimulation for major depression: Coil design and neuroanatomical variability considerations," *Eur. Neuropsychopharmacology*, vol. 45, pp. 73–88, Apr. 2021.

[25] M. Lu and S. Ueno, "Computational study toward deep transcranial magnetic stimulation using coaxial circular coils," *IEEE Trans. Biomed. Eng.*, vol. 62, no. 12, pp. 2911–2919, Dec. 2015.

[26] P. Rastogi, E. G. Lee, R. L. Hadimani, and D. C. Jiles, "Transcranial magnetic stimulation: Development of a novel deep-brain triple-halo coil," *IEEE Magn. Lett.*, vol. 10, pp. 1–5, 2019.

[27] D.-H. Kim, G. E. Georghiou, and C. Won, "Improved field localization in transcranial magnetic stimulation of the brain with the utilization of a conductive shield plate in the stimulator," *IEEE Trans. Biomed. Eng.*, vol. 53, no. 4, pp. 720–725, Apr. 2006, doi: 10.1109/tbme.2006.870244.

[28] E. G. Lee, W. Duffy, R. L. Hadimani, M. Waris, W. Siddiqui, F. Islam, M. Rajamani, R. Nathan, and D. C. Jiles, "Investigational effect of brain-scalp distance on the efficacy of transcranial magnetic stimulation treatment in depression," *IEEE Trans. Magn.*, vol. 52, no. 7, pp. 1–4, Jul. 2016.

[29] Y.-W. Lu and M. Lu, "Comparison of induced fields in virtual human and rat heads by transcranial magnetic stimulation," *BioMed Res. Int.*, vol. 2018, pp. 1–8, Dec. 2018.

[30] C. Zhao, S. Zhang, Z. Liu, and T. Yin, "Simulation study to improve focalization of a figure eight coil by using a conductive shield plate and a ferromagnetic block," *IEEE Trans. Neural Syst. Rehabil. Eng.*, vol. 23, no. 4, pp. 529–537, Jul. 2015.

[31] S. Fiocchi, M. Parazzini, I. Liorni, Y. Roth, A. Zangen, and P. Ravazzani, "Deep transcranial magnetic stimulation for the treatment of neuropsychiatric disorders in elderly people: Electric field assessment," in *Proc. Int. Conf. Electromagn. Adv. Appl. (ICEAA)*, Sep. 2015, pp. 448–451.

[32] M. Parazzini, S. Fiocchi, E. Chiaramello, Y. Roth, A. Zangen, and P. Ravazzani, "Electric field estimation of deep transcranial magnetic stimulation clinically used for the treatment of neuropsychiatric disorders in anatomical head models," *Med. Eng. Phys.*, vol. 43, pp. 30–38, May 2017.

[33] M. Ali, P. Siarry, and M. Pant, "An efficient differential evolution based algorithm for solving multi-objective optimization problems," *Eur. J. Oper. Res.*, vol. 217, pp. 404–416, Sep. 2011.

[34] Y. L. Lv, T. Peng, G. B. Wang, T. H. Ding, X. T. Han, Y. Pan, and L. Li, "Magnet design and analysis of a 40 Tesla long pulse system energized by a battery bank," *J. Low Temp. Phys.*, vol. 170, nos. 5–6, pp. 475–480, Mar. 2013.

[35] J. Ruohonen, J. Virtanen, and R. J. Ilmoniemi, "Coil optimization for magnetic brain stimulation," *Ann. Biomed. Eng.*, vol. 25, no. 5, pp. 840–849, Sep. 1997.

[36] L. Li, T. Peng, H. Ding, X. Han, T. Ding, L. Qiu, Y. Lv, Y. Song, X. Duan, F. Herlach, and Y. Pan, "The development of high performance pulsed magnets of the prototype facility of WHMFC," *IEEE Trans. Appl. Supercond.*, vol. 20, no. 3, pp. 676–679, Jun. 2010.

[37] T. Peng, Q. Q. Sun, X. Zhang, Q. Xu, H. X. Xiao, F. Herlach, Y. Pan, and L. Li, "Design and performance of the first dual-coil magnet at the Wuhan national high magnetic field center," *J. Low Temp. Phys.*, vol. 170, nos. 5–6, pp. 463–468, Mar. 2013.

XIAO FANG received the B.S. degree in electrical engineering from Hunan University, Changsha, China, in 2015, and the Ph.D. degree in electrical engineering from Wuhan National High Magnetic Field Center (WHMFC), Huazhong University of Science and Technology (HUST), Wuhan, China, in 2020.

She is currently an Associate Professor with the College of Nuclear Technology and Automation Engineering, Chengdu University of Technology. She is also a joint Postdoctoral Fellow with the Clinical Hospital of Chengdu Brain Science Institute, MOE Key Laboratory for Neuroinformation, University of Electronic Science and Technology of China (UESTC), and the School of Life Science and Technology, UESTC. Her current research interests include bio-electromagnetic stimulation technology, pulsed power technology, magnet, and power supply design technology.

XIAO XIANG LI received the B.S. degree in electrical engineering and its automation from Wuhan University of Technology, in 2015, and the Ph.D. degree in electrical engineering from Huazhong University of Science and Technology (HUST), Wuhan, China, in 2020.

He is currently a Postdoctoral Fellow with the School of Materials Science and Engineering, HUST. His research interests include magnetic pulse welding, electromagnetic forming, and applications of high magnetic fields.

HAI LIAN JING received the B.S. degree in electrical engineering and automation from Xi'an Polytechnic University, Xi'an, China, and the Ph.D. degree in marine machinery and systems from Tokyo University of Marine Science and Technology, Tokyo, Japan, in 2017.

She is currently with Chengdu University of Technology, Chengdu, China. Her research interests include superconducting motor design, novel power transmission, and superconducting magnetic levitation.

WEI LIU received the B.S. degree in electrical engineering and automation and the Ph.D. degree in transportation information engineering and control from Southwest Jiaotong University, Chengdu, China, in 2006 and 2011, respectively.

He is currently an Associate Professor with the College of Nuclear Technology and Automation Engineering, Chengdu University of Technology (CDUT). His research interests include electric power transmission technology, superconducting technology, and magnetic levitation technology.

TAO ZHANG received the B.S. and M.S. degrees from Shanghai Jiao Tong University, Shanghai, China, in 1996 and 1999, respectively, and the Ph.D. degree in mechanical engineering from Florida State University, in 2004.

From 2005 to 2012, he was a Senior Scientist with the General Electric (GE) Global Research Center. Since 2012, he has been the Chief Technology Officer and the Vice President of Alltech Medical System, China. He is currently a Professor with the School of Life Science and Technology, University of Electronic Science and Technology of China (UESTC). He held over 20 patents and has published over 30 technical articles. His research interests include magnetic resonance imaging (MRI) system technologies and its clinical applications, MRI system hardware development, and the applications of MRI techniques in neuroscience and brain research.

SHUANG ZHANG (Senior Member, IEEE) received the B.S. degree in mathematics and applied mathematics from Neijiang Normal University, Neijiang, China, in 2007, the M.S. degree in control engineering from the Institute of Optics and Electronics, Chinese Academy of Sciences, Chengdu, and the Ph.D. degree in electrical and electronic engineering from the University of Macau, Macau, China, in 2019.

He has been an Associate Professor with the School of Artificial Intelligence, Neijiang Normal University, and a Postdoctoral Researcher with the School of Life Science and Technology, University of Electronic Science and Technology of China (UESTC). His current research interests include human body communication, digital signal processing, body sensor networks, and neuromodulation.

• • •